

Bioorthogonal chemical imaging of metabolic changes during epithelial–mesenchymal transition of cancer cells by stimulated Raman scattering microscopy

Luyuan Zhang
Wei Min

Bioorthogonal chemical imaging of metabolic changes during epithelial–mesenchymal transition of cancer cells by stimulated Raman scattering microscopy

Luyuan Zhang^a and Wei Min^{a,b,*}

^aColumbia University, Department of Chemistry, New York, New York, United States

^bColumbia University, Kavli Institute for Brain Science, New York, New York, United States

Abstract. Study of metabolic changes during epithelial–mesenchymal transition (EMT) of cancer cells is important for basic understanding and therapeutic management of cancer progression. We here used metabolic labeling and stimulated Raman scattering (SRS) microscopy, a strategy of bioorthogonal chemical imaging, to directly visualize changes in anabolic metabolism during cancer EMT at a single-cell level. MCF-7 breast cancer cell is employed as a model system. Four types of metabolites (amino acids, glucose, fatty acids, and choline) are labeled with either deuterium or alkyne ($C \equiv C$) tag. Their intracellular incorporations into MCF-7 cells before or after EMT are visualized by SRS imaging targeted at the signature vibration frequency of C–D or $C \equiv C$ bonds. Overall, after EMT, anabolism of amino acids, glucose, and choline is less active, reflecting slower protein and membrane synthesis in mesenchymal cells. Interestingly, we also observed less incorporation of glucose and palmitate acids into membrane lipids, but more of them into lipid droplets in mesenchymal cells. This result indicates that, although mesenchymal cells synthesize fewer membrane lipids, they are actively storing energy into lipid droplets, either through *de novo* lipogenesis from glucose or direct scavenging of exogenous free fatty acids. Hence, metabolic labeling coupled with SRS can be a straightforward method in imaging cancer metabolism. © 2017 Society of Photo-Optical Instrumentation Engineers (SPIE) [DOI: 10.1117/1.JBO.22.10.106010]

Keywords: stimulated Raman scattering microscopy; chemical imaging; epithelial–mesenchymal transition; cancer metabolism.

Paper 170457R received Jul. 12, 2017; accepted for publication Sep. 27, 2017; published online Oct. 17, 2017.

1 Introduction

The epithelial–mesenchymal transition (EMT) is a process in which epithelial cells dedifferentiate to become mesenchymal cells.¹ It is an essential step in embryonic development, wound healing, and cancer metastasis. Regarding the role of EMT in cancer, metastasis is the primary cause of death of cancer patients.² To metastasize, stationary epithelial cancer cells switch off expression of epithelial markers such as E-cadherin and lose epithelial characteristics such as cell–cell adhesion and polarity. Meanwhile, cells turn on expression of mesenchymal markers such as vimentin and acquire a mesenchymal morphology and ability to migrate and invade.^{3,4}

Cancer cells in general have elevated anabolic metabolism,^{3,5} in order to synthesize cellular components for aberrant proliferation. While protein synthesis is tightly controlled in normal cells, this process is dysregulated in cancer cells, leading to fast and uncontrolled protein synthesis.⁶ Glucose uptake is also generally elevated, in the presence or absence of oxygen (i.e., the Warburg effect).⁷ The uptaken glucose is believed to serve a variety of functions, including providing building blocks for cell mass synthesis, energy production, redox balance, and lactate secretion.⁸ Lipogenesis is also upregulated in cancer cells. This includes both *de novo* lipogenesis from glucose and direct scavenging of exogenous free fatty acids from surroundings.^{9–11}

Although elevated anabolism in cancer cells is generally accepted, metabolic changes during cancer EMT is not well studied. A few recent works have shed light on this topic, mainly through analysis of gene expression. During EMT, cancer cell protein synthesis is quickly inhibited on loss of cell–cell adhesion to preserve ATP, because protein synthesis consumes a large amount of it.¹² In both pancreatic cancer and breast cancer cells, increased expressions are observed for glucose transporters, lactate dehydrogenase A, and lactate exporter MCT4.^{13,14} Pyruvate entry into the TCA cycle is increased due to decreased activity of pyruvate dehydrogenase kinase 4.¹⁵ Oxidative phosphorylation is increased to consume more glucose for ATP production to support mesenchymal cell motility.¹⁶ Glucose anabolism in the pentose phosphate pathway, serine biosynthetic pathway, gluconeogenesis, and *de novo* lipogenesis is all decreased.^{14,17} Synthesis of phosphatidylcholine, an important component of membrane lipids, seems slower in mesenchymal cells.¹⁸ Expression of fatty acid translocase is increased during EMT, suggesting direct scavenging activity.^{18,19} Together, these results suggest that mesenchymal cells might exhibit faster catabolism and slower anabolism than the epithelial counterpart.

Although the previous work on gene expression provides important insight into metabolic changes during cancer EMT, a direct visualization of the relevant metabolites is lacking, especially at the single-cell level. We here directly compared various metabolisms in the epithelial and mesenchymal cells of the

*Address all correspondence to: Wei Min, E-mail: wm2256@columbia.edu

breast cancer cell MCF-7 through stimulated Raman scattering (SRS) microscopy, using deuterium or alkyne tag-labeled amino acids, glucose, choline, and fatty acids. Vibrational imaging by SRS is a rapidly growing field.^{20–24} It is becoming the most powerful vibrational microscopy for biology, owing to its superb sensitivity, imaging speed, three-dimensional optical sectioning, Raman spectral fidelity, a strict linear concentration dependence, straightforward image interpretation, and quantification.^{20–28} Recently, a new bioorthogonal imaging strategy is emerging, by introducing vibrational tags such as deuterium or alkyne labels to small biomolecules.^{29–32} Through deuterium labeling in amino acids, glucose, cholesterol, and fatty acids, SRS microscopy was applied to visualize protein synthesis,³² *de novo* lipogenesis,³³ intracellular cholesterol storage,³⁴ and metabolic activity in live tissues.^{35,36} Through alkyne labeling of glucose, choline, nucleic acids, and fatty acids, SRS microscopy was applied to study the metabolism of glucose uptake,³⁷ choline metabolism,³¹ cell proliferation,^{31,35} and membrane synthesis.³¹

In this work, we employed deuterium-labeled glucose (D7-Glc), deuterium-labeled amino acids (CD-AA), deuterium-labeled palmitate acid (d31-PA), and alkyne-labeled choline (propargylcholine) to directly study glucose metabolism, protein synthesis, fatty acid metabolism, and choline metabolism, respectively, during EMT of the MCF-7 cell model. Slower protein synthesis and membrane synthesis are observed after EMT. Interestingly, new information regarding the metabolism of lipid droplets has been revealed in mesenchymal cells.

2 Materials and Methods

2.1 Stimulated Raman Scattering Microscopy

All laser beams are produced by a custom-modified laser system (picoEMERALD, Applied Physics & Electronics, Inc.). A fundamental 1064-nm Stokes laser (6-ps pulse width) is generated at 80-MHz repetition rate, and its intensity is modulated sinusoidally by an electro-optic modulator at 8 MHz with >90% modulation depth. A mode-locked pump beam (5- to 6-ps pulse width) is produced by a built-in optical parametric oscillator to have a tunable range of 720 to 990 nm. Both laser beams are coupled into an inverted laser-scanning multiphoton microscope (FV1200MPE, Olympus) with optimized near-IR throughput. The spatial and temporal overlapping of the pump and Stokes beam are achieved using two dichroic mirrors and a delay stage inside the laser system based on the heavy water SRS signal. A 25 \times water objective (XLPlan N, 1.05 N.A. MP, Olympus) with high near-IR transmission is used to image all samples. The beam sizes of the pump and Stokes laser are adjusted to match the backaperture of the objective. After the sample in the forward-transmitted direction, a high N.A. condenser lens (oil immersion, 1.4 N.A., Olympus) collects both beams in Kohler illumination with high efficiency. Beam motion from laser-scanning is descanned with a telescope and a high O.D. bandpass filter (890/220 CARS, Chroma Technology) is used to block the Stokes beam completely and passes only the pump beam.

A large-area (10 mm \times 10 mm) silicon photodiode (FDS1010, Thorlabs) is reverse-biased with a 64-DC voltage to maximize the saturation threshold and response bandwidth and is used to collect the entire pump beam. The output photocurrent is electronically filtered to remove both the 80-MHz component of laser pulsing and low frequency fluctuations

from scanning motion using an 8-MHz electronic bandpass filter (KR 2724, KR electronics) and is terminated with 50 Ω before entering a radio frequency lock-in amplifier (SR844, Stanford Research Systems). The corresponding voltage signal is demodulated at the reference frequency to extract the stimulated Raman loss signal from the pump beam with near short-noise-limited sensitivity. SRS images are generated by inputting the in-phase signal at the X channel of the lock-in amplifier to the analog interface box (FV10-ANALOG) of the microscope at each pixel and scanning across the whole field of view. \sim 120-mW pump beam and \sim 150-mW Stokes beam, measured after the 25 \times water objective, are used to image the sample at all frequencies. The demodulation time constant is 30 μ s and the imaging pixel dwell time is 100 μ s with \sim 26 s/frame (512 \times 512 pixels) for all images. For study of metabolic changes during EMT using metabolic labels, epithelial and mesenchymal cells are imaged under the same SRS microscopy, with the same laser powers and acquisition parameters. To quantitatively compare the metabolism, we summed up the C-D or alkyne SRS intensities of the two-dimensional images of single cells using the software ImageJ. For each metabolic label, more than 30 each of epithelial and mesenchymal cells are calculated and compared to achieve statistical significance.

2.2 Metabolic Labeling

All deuterium-labeled amino acids (CD-AA), palmitate acid (d31-PA), and D-glucose (D7-Glc) were purchased from Cambridge Isotope. For deuterium-labeled amino acids mediums, we prepared EMEM medium from scratch according to a recipe on atcc.org, replacing all amino acids with their deuterium-labeled version. For the d31-PA incorporation experiment, we simply added 50- μ M d31-PA into the complete growth medium of MCF-7. For the D7-Glc incorporation experiment, we prepared EMEM medium from scratch according to a recipe on atcc.org, replacing regular D-glucose with deuterium-labeled D7-D-glucose. Propargylcholine was synthesized in house according to a previously reported method.^{31,38} For the propargylcholine incorporation experiment, we simply added 1-mM propargylcholine into the complete growth medium of MCF-7. For each labeling experiment, epithelial and mesenchymal cells were cultured in the same media with the same duration.

2.3 Cell Culture

The MCF-7 cell line was purchased from atcc.org. Cells were grown in a complete medium containing EMEM, 10 μ g/ml insulin, 10% FBS, and 1% P&S. For imaging, cells were seeded into plates containing cover slides with a density of 2×10^4 cell/cm² and allowed to proliferate for 1 to 2 days. We used the StemXVivo EMT-inducing media supplement from R&D systems. To induce EMT, the complete medium in culture wells was replaced with EMEM, 10 μ g/ml insulin and 1 \times inducing supplement. The inducing medium was replaced with fresh inducing medium every 3 days. After 5 to 8 days, MCF-7 cells became mesenchymal, and the inducing medium was replaced with EMEM containing 10 μ g/ml insulin, 10% FBS, and metabolic labels containing C-D bond or C \equiv C bond. We allowed 2 days of incorporation of the metabolic labels, and then imaged cells live with the SRS microscope. For comparison, epithelial and mesenchymal MCF-7 cells were studied in parallel.

2.4 Immunofluorescence

Primary antibodies rabbit anti-vimentin and mouse anti-E-cadherin, and secondary antibodies goat-anti-rabbit antibody conjugated with Alexa488 and goat-anti-mouse antibody conjugated with Alexa647 were all purchased from abcam.com. Epithelial and mesenchymal MCF-7 cells were grown in a glass coverslip and stained with primary antibody at 4°C overnight then stained with secondary antibody for 1 h at room temperature, according to the manufacturer's instruction. Then, vimentin and E-cadherin distribution were imaged with fluorescence from excitation at 488 and 647 nm, respectively. Cell nuclei were stained with NucBlue from ThermoFisher Scientific and imaged with 2-photon excitation at 780 nm.

3 Results

Spontaneous Raman spectra of MCF-7 cells grown in unlabeled or labeled mediums are shown in Fig. 1. Without any labels (bottom gray), the spectrum has a silent region in 1800 to 2400 cm^{-1} where no Raman peaks from other biological

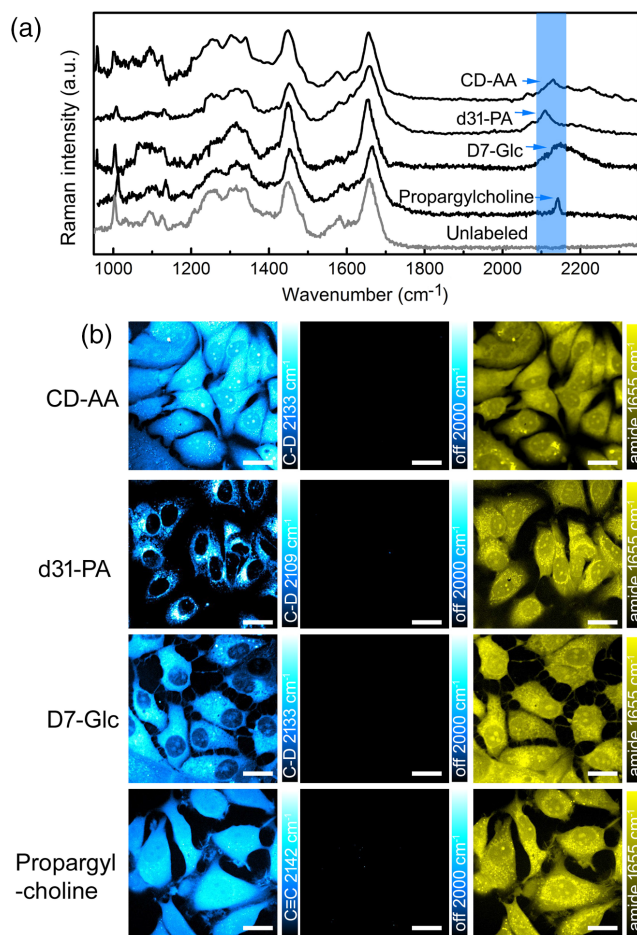


Fig. 1 (a) Spontaneous Raman spectra of MCF-7 cells cultured with metabolic labels. MCF-7 cells cultured in regular medium do not have any Raman peak in 1800 to 2400 cm^{-1} (gray curve on bottom). Cells cultured in deuterium- or alkyne-labeled metabolites show Raman peaks that are signature of the label (cyan shade). (b) Representative SRS images of MCF-7 cells cultured in mediums with metabolic labels. Left, incorporated metabolites. Middle, cell silent region that is far away from Raman peak of metabolic labels. Right, SRS images at 1655 cm^{-1} from amide vibration that represent intrinsic protein pool. Scale bars, 50 μm .

molecules exist. After culturing in mediums supplemented with labeled metabolites, Raman peaks from incorporated metabolic labels appear in the silent region. Metabolites from deuterium-labeled glucose, amino acids, and palmitate acids all have broad Raman peaks, ranging from 2050 to 2300 cm^{-1} , which are from the C-D bonds vibration. For SRS imaging, we pick the highest peaks for each label, i.e., 2133 cm^{-1} for D7-Glc and CD-AA, and 2109 cm^{-1} for d31-PA. In contrast, propargylcholine has a signature sharp Raman peak at 2142 cm^{-1} from the C \equiv C alkyne tag.

Representative SRS images of MCF-7 cultured in the labeled mediums are also shown in Fig. 1(b). Left panels are SRS images targeted at the signature frequencies of the C-D or C \equiv C vibrations. When the frequency is moved away to 2000 cm^{-1} , where the metabolic labels do not show any Raman signatures, no SRS signals can be detected (middle panels). SRS images of the same cells at a frequency of 1655 cm^{-1} (amide vibration attributed mainly to proteins) show a strong signal from the total protein pool illustrating the cell morphology (right panels).

We next aim to study metabolic changes during EMT of MCF-7 cells. We induced EMT using a standard EMT inducer from R&D systems. We first validated the method by immunofluorescence staining of the cells before and after EMT, using antibodies for E-cadherin and vimentin, which are well-established markers for epithelial and mesenchymal cells, respectively. The images are shown in Fig. 2. As expected, MCF-7 loses E-cadherin and acquires vimentin after EMT. We then followed this validated protocol to induce EMT of MCF-7 for the study of metabolism here. Epithelial and mesenchymal MCF-7 cells are cultured in mediums with d31-PA, D7-Glc, CD-AA, or propargylcholine for 1 to 2 days. SRS images were acquired for both types of cells, and they are shown in Figs. 3–6.

In Fig. 3, before EMT, CD-AA showed bright C-D SRS intensity, reflecting rapid protein synthesis in epithelial cells. The bright puncta are from nucleoli with fast protein turnover.³² After EMT, C-D SRS intensity in mesenchymal cells is visually darker than epithelial cells, indicating reduced protein synthesis after EMT. Analysis of the images revealed a reduction of around 30% in CD-AA incorporation. This is consistent with reports from other groups that protein synthesis¹² is slowed down during cancer EMT. Meanwhile, cells also acquire a large amount of lipid droplets, which appear as bright puncta in the CH_2 lipid channel at 2845 cm^{-1} . The average number of lipid droplets increased from less than 10 per cell in epithelial cells to around 50 per cell in mesenchymal cells.

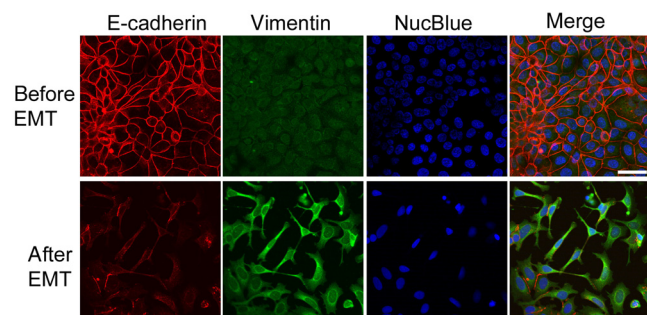


Fig. 2 Immunofluorescence of MCF-7 shows cells undergo epithelial–mesenchymal transition. Before EMT, cells have bright E-cadherin (red) staining but weak vimentin (green) staining. After EMT, E-cadherin expression decreased while vimentin expression increased. Scale bars, 50 μm .

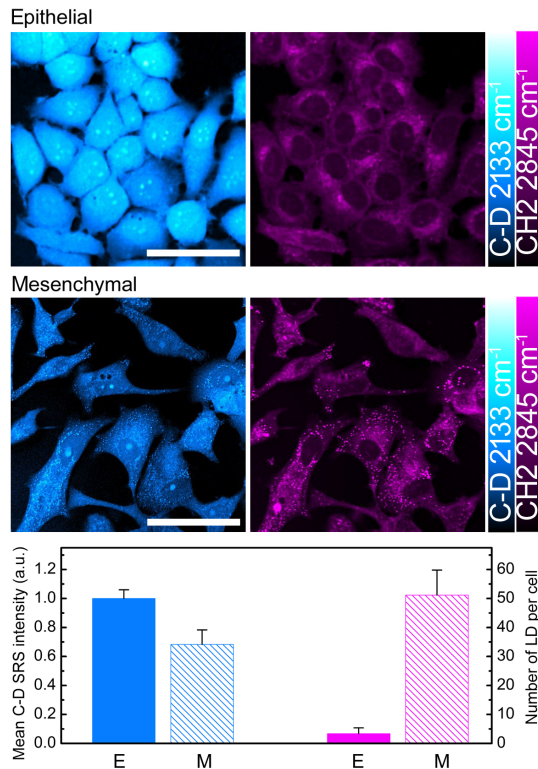


Fig. 3 CD-AA incorporation in MCF-7 during EMT. C-D SRS images of mesenchymal cells are darker than epithelial cells, meanwhile mesenchymal cells have lots of lipid droplets, which appear as bright puncta in both C-D and CH₂ SRS images. Analysis of image reveals that C-D incorporation decreased by ~30% during EMT, reflecting slower protein synthesis. Number of intracellular lipid droplets increased from less than 10 to around 50. Scale bar, 50 μ m.

Figure 4 shows choline metabolism during EMT of MCF-7 cells. The signal of propargylcholine reflects the synthesis activity of choline phospholipids which is the main component of biological membrane.^{31,38} Before EMT, the alkyne tag from propargylcholine shows bright SRS images at its peak Raman frequency 2142 cm^{-1} , across the whole cell. This reflects active membrane synthesis in rapidly proliferating epithelial cells. After EMT, however, SRS images of the alkyne tag become much dimmer, and the majority of propargylcholine concentrates in the endoplasmic reticulum (ER) region. This reflects that there is less membrane synthesis in mesenchymal cells, which does not proliferate as fast as epithelial cells, and choline is synthesized only into regions where lipids turnover is fast, such as ER. Analysis of image intensity reveals the incorporation of choline reduced by around 80% after EMT. Our imaging result is consistent with reports that choline anabolic metabolism¹⁸ is slowed down during cancer EMT.

Figure 5 shows D7-Glc metabolism during MCF-7 EMT. Glucose can be synthesized into proteins, DNA, and lipids inside cells. In epithelial cells, it appears that glucose is incorporated into both proteins and membrane lipids, reflecting fast protein and membrane synthesis in rapidly proliferating epithelial cells. In mesenchymal cells, however, the overall C-D signal is weaker across cytoplasm than epithelial cells, and it is concentrated in bright droplets (indicated by green arrows). These bright droplets also appear on the CH₂ SRS channel at a frequency of 2845 cm^{-1} (indicated by green arrows). Therefore, in mesenchymal cells, apart from being synthesized

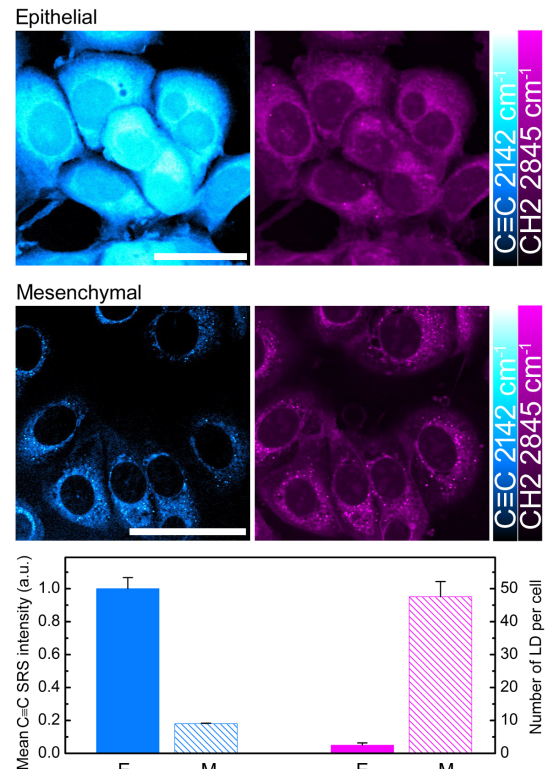


Fig. 4 Propargylcholine incorporation in MCF-7 during EMT. C=C SRS images of mesenchymal cells are darker than epithelial cells. Meanwhile mesenchymal cells have lots of lipid droplets, which appear as bright puncta in both C=C and CH₂ SRS images. Analysis of image reveals that C-D incorporation decreased by ~80% during EMT, reflecting slower membrane synthesis. Number of intracellular lipid droplets increased from less than 10 to around 50. Scale bar, 50 μ m.

into membrane lipids, glucose is also metabolized and stored into lipid droplets as energy storage. SRS intensity analysis revealed that total incorporation of the C-D from D7-Glc is reduced by around 50% during MCF-7 EMT, and the average number of lipid droplets increased from less than 10 per cell in epithelial cells to around 50 per cell in mesenchymal cells.

Free fatty acids are important building blocks for lipid synthesis for proliferating cells.³⁹ Figure 6 shows the incorporation result of d31-PA. In epithelial cells, the distribution of the C-D SRS signal from d31-PA resembles the SRS signal at 2845 cm^{-1} of CH₂ vibration mainly from lipids. Hence, in epithelial cells, d31-PA is actively taken up by cells and incorporated into membrane lipids, reflecting fast membrane synthesis in rapidly proliferating epithelial cells from the scavenging pathway. In mesenchymal cells, membrane C-D SRS is weaker compared with epithelial cells. Moreover, C-D appeared in the bright lipid droplets (indicated by green arrows). These droplets colocalize with lipid droplets in the CH₂ channel (indicated by green arrows). SRS intensity analysis of individual cells reveals that, when not considering lipid droplets, d31-PA incorporation into membrane lipids is decreased by around 20% during EMT. However, when lipid droplets are included, the overall intracellular C-D derived from d31-PA increased by around 20% during EMT. Therefore, our data revealed a previously unknown phenomenon: after EMT, membrane synthesis from scavenged free fatty acid is decreased likely due to the decreased cell proliferation, but the overall fatty acids uptake is increased, and the

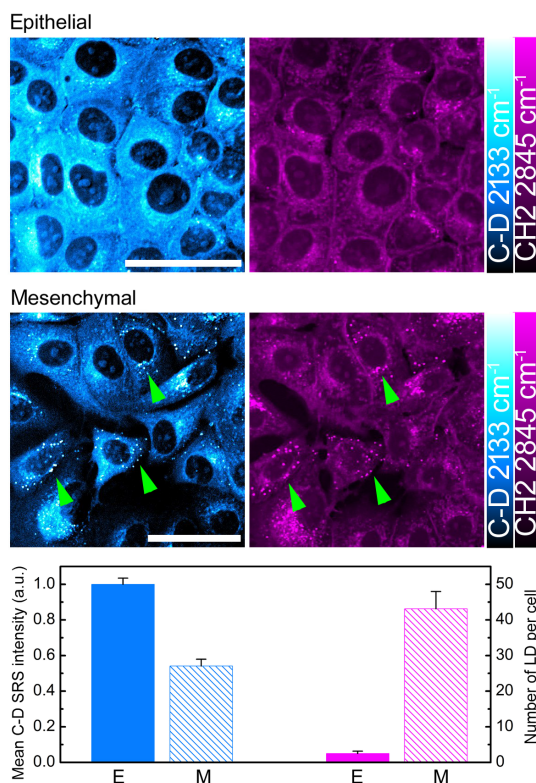


Fig. 5 D7-Glc incorporation in MCF-7 during EMT. C-D SRS images of mesenchymal cells are darker than epithelial cells. Meanwhile mesenchymal cells have lots of lipid droplets, which appear as bright puncta in both C-D and CH₂ SRS images. Analysis of image reveals that C-D incorporation decreased by ~50% during EMT, reflecting slower biomass synthesis. Number of intracellular lipid droplets increased from less than 10 to around 50. Scale bar, 50 μ m.

majority of it is converted to triglyceride (which is the major component of lipid droplets) and stored as energy in the form of lipid droplets.

4 Discussion and Conclusion

Epithelial–mesenchymal transition is a critical step in cancer progression and metastasis. While the metabolism change during EMT has been studied through analysis of mRNA and protein levels of key metabolic enzymes, direct microscopic imaging of metabolism at the single-cell level is challenging, primarily due to lack of imaging probes. By using metabolites that are labeled with distinct vibration tags, here we are able to visualize the metabolism of various small metabolites such as fatty acid, amino acids, glucose, and choline. We found that the incorporation rates of amino acids, choline, and glucose are all decreased by various amounts after EMT. These results indicate the need of mesenchymal cells to restrict biosynthesis of proteins and lipids (which consumes energy) and to preserve energy for its migration and invasion.

Our chemical imaging approach also revealed previous unknown information. The change of glucose metabolism during EMT is not only in its overall incorporation into biomass but also where it is incorporated into (Fig. 5). In epithelial cells, C-D from D7-Glc shows homogeneous distribution across cytoplasm, indicating its incorporation into proteins and membrane lipids. In mesenchymal cells, *de novo* synthesis from glucose is severely reduced, reflecting the stalled proliferation of

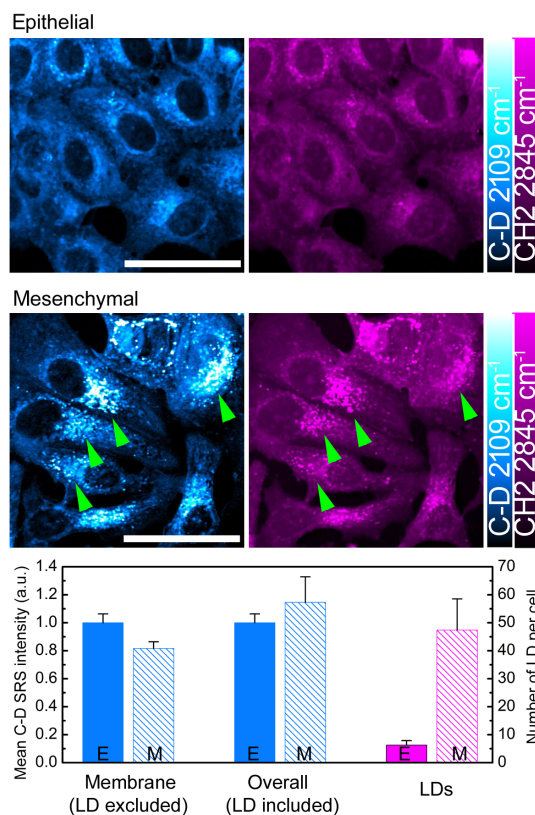


Fig. 6 d31-PA incorporation in MCF-7 during EMT. In epithelial cells, d31-PA are mainly incorporated into membrane lipids, as evidenced by the resemblance to CH₂ of lipids. In mesenchymal cells, d31-PA is also largely incorporated into lipid droplets, which also appear in CH₂ lipids channel. Analysis of C-D SRS signal of individual cells reveals that without considering lipid droplets, d31-PA incorporation into membrane lipids is less after EMT. When all lipid droplets are included, overall C-D SRS is higher after EMT. Number of intracellular lipid droplets increased from less than 10 to around 50. Scale bar, 50 μ m.

mesenchymal cells. However, synthesis of triglycerides in lipid droplets from glucose is obviously increased relative to epithelial cells. Lipid droplet is a form of energy storage, and our result indicates that mesenchymal cells store more energy, and one way to do it is through *de novo* lipogenesis from glucose. Along a similar line, d31-PA metabolism changes not only quantitatively but also qualitatively (Fig. 6). Epithelial cells mainly build free palmitic acids into membrane lipids, reflecting its needs for fatty acid to sustain fast proliferation. Mesenchymal cells uptake even more fatty acid, although it does not need fatty acid for lipid synthesis. The uptaken fatty acids are not built into membrane but into lipid droplets. Together, the direct imaging approach taken in this study is indispensable in unraveling this microscopic information at subcellular level.

Regarding lipid droplets, here we observed their accumulation in mesenchymal cells, both from the *de novo* lipogenesis pathway (Fig. 5) and from the fatty acid scavenging pathway (Fig. 6). Recently, the lipid droplet has emerged as an important player in cancer biology.^{40–42} Accumulation of lipid droplets was also observed in prostate cancer cell EMT.⁴³ More malignant tumor tissues tend to accumulate more lipid droplets.^{40,44} Inhibition of fatty acid synthase reverses the EMT and malignancy of breast cancer and glioblastoma cancer.^{45,46} Together, it seems that lipid droplets might play important functions in

maintaining malignancy and mesenchymal phenotype of cancer cells.

Disclosures

The authors have no relevant financial interests in this article and no potential conflicts of interest to disclose.

Acknowledgments

W. M. acknowledges support from an NIH Director's New Innovator Award (1DP2EB016573), R01 (EB020892), the US Army Research Office (W911NF-12-1-0594), the Alfred P. Sloan Foundation, and the Camille and Henry Dreyfus Foundation.

References

- S. Lamouille, J. Xu, and R. Derynck, "Molecular mechanisms of epithelial-mesenchymal transition," *Nat. Rev. Mol. Cell Biol.* **15**, 178–196 (2014).
- P. Mehlen and A. Puisieux, "Metastasis: a question of life or death," *Nat. Rev. Cancer* **6**, 449–458 (2006).
- L. N. Li and W. L. Li, "Epithelial-mesenchymal transition in human cancer: comprehensive reprogramming of metabolism, epigenetics, and differentiation," *Pharmacol. Ther.* **150**, 33–46 (2015).
- W. L. Tam and R. A. Weinberg, "The epigenetics of epithelial-mesenchymal plasticity in cancer," *Nat. Med.* **19**, 1438–1449 (2013).
- S. C. Dolfi et al., "The metabolic demands of cancer cells are coupled to their size and protein synthesis rates," *Cancer Metab.* **1**, 20 (2013).
- M. Bhat et al., "Targeting the translation machinery in cancer," *Nat. Rev. Drug Discovery* **14**, 261–278 (2015).
- O. Warburg, F. Wind, and E. Negelein, "The metabolism of tumors in the body," *J. Gen. Physiol.* **8**, 519–530 (1927).
- M. V. Liberti and J. W. Locasale, "The Warburg Effect: how does it benefit cancer cells?" *Trends Biochem. Sci.* **41**, 211–218 (2016).
- V. W. Daniëls et al., "Cancer cells differentially activate and thrive on de novo lipid synthesis pathways in a low-lipid environment," *PLoS One* **9**, e106913 (2014).
- C.-H. Yao et al., "Exogenous fatty acids are the preferred source of membrane lipids in proliferating fibroblasts," *Cell Chem. Biol.* **23**, 483–493 (2016).
- F. P. Kuhajda, "Fatty-acid synthase and human cancer: new perspectives on its role in tumor biology," *Nutrition* **16**, 202–208 (2000).
- T. L. Ng et al., "The AMPK stress response pathway mediates anoikis resistance through inhibition of mTOR and suppression of protein synthesis," *Cell Death Differ.* **19**, 501–510 (2011).
- M. H. Liu et al., "Epithelial-mesenchymal transition induction is associated with augmented glucose uptake and lactate production in pancreatic ductal adenocarcinoma," *Cancer Metab.* **4**, 19 (2016).
- Y. Kondaveeti, I. K. G. Reed, and B. A. White, "Epithelial-mesenchymal transition induces similar metabolic alterations in two independent breast cancer cell lines," *Cancer Lett.* **364**, 44–58 (2015).
- Y. Sun et al., "Metabolic and transcriptional profiling reveals pyruvate dehydrogenase kinase 4 as a mediator of epithelial-mesenchymal transition and drug resistance in tumor cells," *Cancer Metab.* **2**, 20 (2014).
- V. S. LeBleu et al., "PGC-1 α mediates mitochondrial biogenesis and oxidative phosphorylation in cancer cells to promote metastasis," *Nat. Cell Biol.* **16**, 992–1003 (2014).
- L. Jiang et al., "Metabolic reprogramming during TGF[β 1]-induced epithelial-to-mesenchymal transition," *Oncogene* **34**, 3908–3916 (2015).
- M. Jechlinger et al., "Expression profiling of epithelial plasticity in tumor progression," *Oncogene* **22**, 7155–7169 (2003).
- A. Nath and C. Chan, "Genetic alterations in fatty acid transport and metabolism genes are associated with metastatic progression and poor prognosis of human cancers," *Sci. Rep.* **6**, 18669 (2016).
- C. H. Camp and M. T. Cicerone, "Chemically sensitive bioimaging with coherent Raman scattering," *Nat. Photonics* **9**, 295–305 (2015).
- J. X. Cheng and X. S. Xie, "Vibrational spectroscopic imaging of living systems: an emerging platform for biology and medicine," *Science* **350**, aaa8870 (2015).
- C. S. Liao and J. X. Cheng, "In situ and in vivo molecular analysis by coherent Raman scattering microscopy," *Annu. Rev. Anal. Chem.* **9**, 69–93 (2016).
- W. Min et al., "Coherent nonlinear optical imaging: beyond fluorescence microscopy," *Annu. Rev. Phys. Chem.* **62**, 507–530.
- C. Krafft et al., "Developments in spontaneous and coherent Raman scattering microscopic imaging for biomedical applications," *Chem. Soc. Rev.* **45**, 1819–1849 (2016).
- A. Einstein, "On the quantum theory of radiation," *Phys. Z.* **18**, 121–128 (1917).
- N. Bloembergen, "Stimulated Raman effect," *Am. J. Phys.* **35**, 989–1023 (1967).
- C. W. Freudiger et al., "Label-free biomedical imaging with high sensitivity by stimulated Raman scattering microscopy," *Science* **322**, 1857–1861 (2008).
- B. G. Saar et al., "Video-rate molecular imaging in vivo with stimulated Raman scattering," *Science* **330**, 1368–1370 (2010).
- L. Wei et al., "Live-cell bioorthogonal chemical imaging: stimulated Raman scattering microscopy of vibrational probes," *Acc. Chem. Res.* **49**, 1494–1502 (2016).
- S. L. Hong et al., "Live-cell stimulated Raman scattering imaging of alkyne-tagged biomolecules," *Angew. Chem. Int. Ed.* **53**, 5827–5831 (2014).
- L. Wei et al., "Live-cell imaging of alkyne-tagged small biomolecules by stimulated Raman scattering," *Nat. Methods* **11**, 410–412 (2014).
- L. Wei et al., "Vibrational imaging of newly synthesized proteins in live cells by stimulated Raman scattering microscopy," *Proc. Natl. Acad. Sci. U. S. A.* **110**, 11226–11231 (2013).
- J. J. Li and J. X. Cheng, "Direct visualization of de novo lipogenesis in single living cells," *Sci. Rep.* **4**, 6807 (2014).
- A. Alfonso-Garcia et al., "D38-cholesterol as a Raman active probe for imaging intracellular cholesterol storage," *J. Biomed. Opt.* **21**, 061003 (2016).
- F. H. Hu et al., "Bioorthogonal chemical imaging of metabolic activities in live mammalian hippocampal tissues with stimulated Raman scattering," *Sci. Rep.* **6**, 39660 (2016).
- L. Wei et al., "Imaging complex protein metabolism in live organisms by stimulated Raman scattering microscopy with isotope labeling," *ACS Chem. Biol.* **10**, 901–908 (2015).
- F. H. Hu et al., "Vibrational imaging of glucose uptake activity in live cells and tissues by stimulated Raman scattering," *Angew. Chem. Int. Ed.* **54**, 9821–9825 (2015).
- C. Y. Jao et al., "Metabolic labeling and direct imaging of choline phospholipids in vivo," *Proc. Natl. Acad. Sci.* **106**, 15332–15337 (2009).
- C.-H. Yao et al., "Exogenous fatty acids are the preferred source of membrane lipids in proliferating fibroblasts," *Cell Chem. Biol.* **23**, 483–493 (2016).
- L. Tirineto et al., "Lipid droplets: a new player in colorectal cancer stem cells unveiled by spectroscopic imaging," *Stem Cells* **33**, 35–44 (2015).
- S. Koizume and Y. Miyagi, "Lipid droplets: a key cellular organelle associated with cancer cell survival under normoxia and hypoxia," *Int. J. Mol. Sci.* **17**(9), E1430 (2016).
- J. Li et al., "Lipid desaturation is a metabolic marker and therapeutic target of ovarian cancer stem cells," *Cell Stem Cell* **20**, 303–314.e305.
- N. Dalmau et al., "Epithelial-to-mesenchymal transition involves triacylglycerol accumulation in DU145 prostate cancer cells," *Mol. Biosyst.* **11**, 3397–3406 (2015).
- S. Yue et al., "Cholesteryl ester accumulation induced by PTEN loss and PI3K/AKT activation underlies human prostate cancer aggressiveness," *Cell Metab.* **19**, 393–406 (2014).
- A. M. Gonzalez-Guerrico et al., "Suppression of endogenous lipogenesis induces reversion of the malignant phenotype and normalized differentiation in breast cancer," *Oncotarget* **7**, 71151–71168 (2016).
- Y. Yasumoto et al., "Inhibition of fatty acid synthase decreases expression of stemness markers in glioma stem cells," *PLoS One* **11**(1), e0147717 (2016).

Luyuan Zhang received her PhD in chemical physics in 2010 from The Ohio State University. She is currently a postdoctoral research

scientist at Columbia University working on imaging abnormal metabolism in morbid animal models. Her research interests are in developing and applying innovative nonlinear Raman microscopy for studies of various cellular activities.

Wei Min graduated from Peking University, China, with a bachelor's degree in 2003. He received his PhD in chemistry from Harvard

University in 2008 with Prof. Sunney Xie. After continuing his postdoctoral work in the Xie group, he joined the Faculty of Department of Chemistry at Columbia University in July 2010. He is currently a professor there, and his research interests focus on developing innovative optical spectroscopy and microscopy technology to address biomedical problems.